

Key requirements for ultraefficient sensitization in hyperfluorescence organic light-emitting diodes

Received: 26 July 2023

Accepted: 18 January 2024

Published online: 13 February 2024

Check for updates

Kleitos Stavrou¹ ✉, Larissa G. Franca, Andrew Danos¹ & Andrew P. Monkman¹ ✉

Blue organic light-emitting diode (OLED) technology requires further advancements, and hyperfluorescent (HF) OLEDs have emerged as a promising solution to address stability and colour-purity concerns. A key factor influencing the performance of HF-OLEDs is Förster resonance energy transfer (FRET). Here we investigate the FRET mechanism in blue HF-OLEDs using contrasting thermally activated delayed fluorescence (TADF) sensitizers. We demonstrate that the molecular structure of the sensitizer profoundly impacts the FRET efficiency, exemplified by the spiro-linked TADF molecule ACRSA, which suppresses the dihedral-angle inhomogeneity and any lower-energy conformers that exhibit minimal FRET to the terminal emitter. Consequently, the FRET efficiency can be optimized to nearly 100%. Further, we demonstrate how the properties of a near-ideal sensitizer diverge from ideal TADF emitters. As a result, blue HF-OLEDs utilizing a greenish sensitizer exhibit a remarkable tripling of external quantum efficiency (~30%) compared with non-HF devices. This new understanding opens avenues for sensitizer design, indicating that green sensitizers can efficiently pump blue terminal emitters, thereby reducing device exciton energies and improving blue OLED stability.

Commercial organic light-emitting diodes (OLEDs) still require better blue emitters^{1,2}. Even today, fluorescent and/or triplet fusion emitters are used for commercial blue OLED pixels, as these materials alone provide acceptable device lifetimes³, despite lower efficiency compared with blue phosphorescent or thermally activated delayed fluorescence (TADF) emitters^{4,5}. The potential benefits of stable higher-performance blue emitters are even more pressing because of newly envisioned OLED display architectures, which exclusively utilize blue pixels with external fluorescent colour conversion layers^{6,7}. These offer ~30% reduction in power consumption, and in the future could save more than 150 TWh in annual global residential electricity consumption (Supplementary Information).

Hyperfluorescent (HF) OLEDs offer ways to achieve this, circumvent the limitations of both TADF or phosphorescent blue emitters,

and using them as sensitizers for separate terminal emitters⁸, but this approach is still relatively immature and not well understood^{9–11}. A high-performance deep-blue ‘triplet-harvesting’ sensitizer with good spectral overlap to a terminal emitter is required, enabling efficient Förster resonance energy transfer (FRET)^{10,12,13}. The broad emission spectra and low radiative rates of a TADF sensitizer can, thus, be compensated for by the fast and narrowband emission from the terminal emitter and 100% triplet excitons are utilized by the former^{14–16}. Concomitantly, we have shown that some green-emitting sensitizers can support blue HF-OLEDs¹⁷. This translates to a lowering of the singlet and triplet energies of all the materials in the emission layer, improving the device stability.

However, many papers report HF-TADF OLEDs with external quantum efficiencies (EQEs) lower than their TADF counterparts^{12,18}. Where

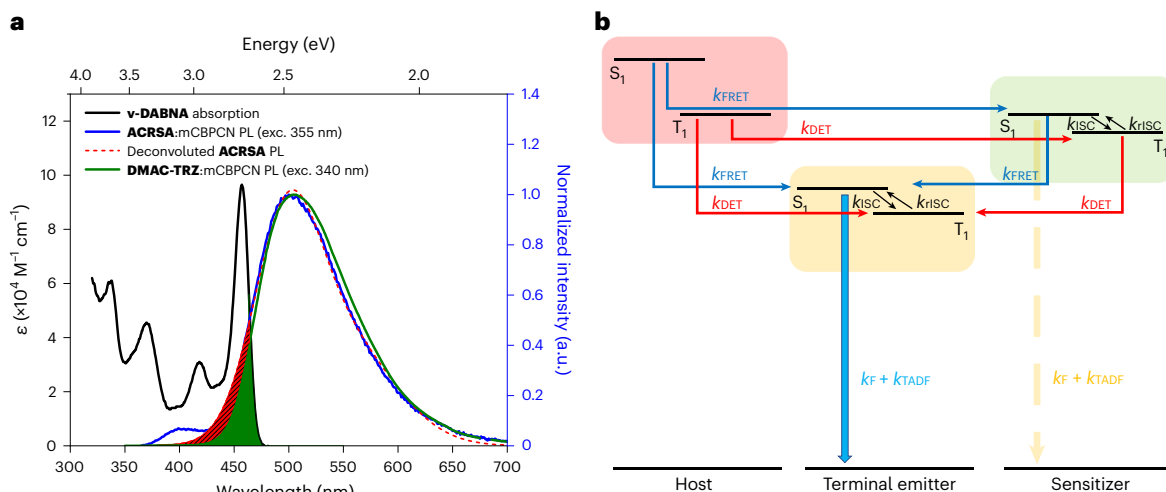


Fig. 1 Sensitizer terminal emitter spectral overlap for FRET and the corresponding energy pathways. **a**, Steady-state absorption of **v-DABNA** in a toluene solution, alongside the PL spectra of **ACRSA:mCBPCN** (10 wt%) and **DMAC-TRZ:mCBPCN** (10 wt%) films, excited at 355 and 340 nm, respectively. **DMAC-TRZ:mCBPCN** films exhibit a strong emission band centred at 500 nm, which we have shown is the ¹CT emission from the highly twisted quasi-equatorial conformer distribution¹⁷. In **ACRSA:mCBPCN**, the broad emission band at

~500 nm is a characteristic of **ACRSA** ¹CT emission in solid-state hosts³⁶; the emission at 400 nm is from the mCBPCN host whose absorption at 340 nm is much stronger compared with that of **ACRSA**. The filled areas are the spectral overlaps between the curves used to calculate the FRET radius. **b**, FRET mechanism in a guest:sensitizer:terminal emitter system. The emission from the sensitizer (yellow arrow) occurs when FRET is less than 100% efficient.

EQEs are higher^{10,19}, no clear pattern or identifiable underlying cause is given. Multiresonance TADF terminal emitters¹⁴ that also harvest triplet excitons yield HF-OLEDs that typically outperform non-HF devices^{20–24}. Along with EQE, in many cases, the HF-OLED efficiency roll-off performance is better, but in some cases, it is worse^{15,24}. In almost all the reports, the ‘best’ TADF emitters are used in pre-optimized OLED stacks with a small concentration of the terminal emitter added to make an HF-OLED—prima facie, a sensible strategy^{12,25–27}. However, the TADF emitter may already be performing at its maximum potential, and the introduction of a terminal emitter opens up additional loss pathways, for example, charge or triplet trapping on the terminal emitter. The terminal emitter can contribute to higher performance through higher photoluminescence quantum yield (PLQY) or improved light out-coupling, but these do not always outweigh the additional losses^{16,28}.

The performance of such best TADF emitters also relies on a delicately balanced highest occupied molecular orbital–lowest unoccupied molecular orbital overlap²⁹. A high overlap will increase the oscillator strength and PLQY (the ratio of radiative and non-radiative decay rates), but is detrimental to triplet-harvesting reverse intersystem crossing rates (k_{rISC}) and vice versa³⁰. Thus, donor–acceptor TADF emitters with the fastest reverse intersystem crossing (rISC) rates but limited PLQYs do not produce high-performance OLEDs and are typically not investigated in HF-OLEDs. Counterintuitively, in HF-OLEDs, the PLQY of the sensitizer is not crucial if the FRET rate (k_{FRET}) outcompetes the non-radiative decay, and instead, the higher k_{rISC} is the most beneficial.

Here we demonstrate extraordinary HF-OLED performance enhancement using TADF sensitizers, which themselves only give moderate non-HF device performance. Starting from our recent work using the high-performance TADF emitter **DMAC-TRZ** as a benchmark^{17,31}, we demonstrate that **ACRSA** (moderate OLED performance) gives HF-OLEDs with an almost tripled EQE_{max} (refs. 10,32). Similar results are also demonstrated with the deeper-blue TADF emitter **AZB-TRZ** (ref. 33), which has fast rISC but low PLQY. Surprisingly, despite the photoluminescence (PL) spectra of **ACRSA** and **DMAC-TRZ** being energetically similar (comparable/factors), **ACRSA** exhibits notably higher FRET efficiency with **v-DABNA**, even compared with the deeper-blue

AZB-TRZ sensitizer, which has better spectral overlap. We demonstrate that this arises because of **ACRSA**’s rigid structure and long-lived excited states, normally a detriment in OLEDs. These findings establish new and unexpected design rules for high-performance HF sensitizers.

Results

Photophysics

The steady-state PL spectra of **ACRSA** and **DMAC-TRZ** at 10 wt% in the 3,3′-di(carbazol-9-yl)-5-cyano-1,1′-biphenyl (mCBPCN) host are shown in Fig. 1. The intrinsic broadness of the **DMAC-TRZ** charge transfer (CT) emission, centred at 500 nm, is due to contributions from different molecular configurations with different donor–acceptor dihedral angles in the film, together with some aggregate emission (Supplementary Fig. 2b)^{34,35}. These contributions are resolved in time-resolved spectra even when FRET to a terminal emitter is active (in this case, **v-DABNA**)^{14,27} (Supplementary Fig. 1c). In **ACRSA**, the absence of dihedral-angle inhomogeneity results in a narrower intrinsic PL spectrum, as evident in the deconvoluted spectra of **ACRSA** (Supplementary Fig. 2a) and as reported previously^{35,36}.

Excluding the mCBPCN contribution to the **ACRSA** PL spectrum, comparing the spectral overlap in the two TADF emitters with **v-DABNA** absorption²⁷, **ACRSA** displays slightly increased spectral overlap because of its higher energy PL onset (Fig. 1, red-filled area), compared to the **DMAC-TRZ** overlap which is highlighted in green. For both emitters, only the blue edge of their emission overlaps with the narrow S_0 – S_1 absorption of **v-DABNA**, but efficient FRET surprisingly still ensues for both materials (although for different reasons, as discussed below). The calculated FRET radii between **v-DABNA** and **ACRSA** or **DMAC-TRZ** are estimated to be 2.8 and 3.2 nm, respectively (Supplementary Information). **ACRSA:v-DABNA** has slightly better spectral overlap but the calculated FRET radius is lower than **DMAC-TRZ:v-DABNA** because the **ACRSA** PLQY is three times smaller.

The FRET dynamics in the two HF systems were investigated using time-resolved emission spectroscopy. For the **ACRSA:mCBPCN** (10 wt%) film (Fig. 2a), three species are identified; mCBPCN, **ACRSA** singlet CT (¹CT) and **ACRSA** excimers (Table 1 lists their lifetimes). The very long ¹CT decay lifetime arises from the highly decoupled

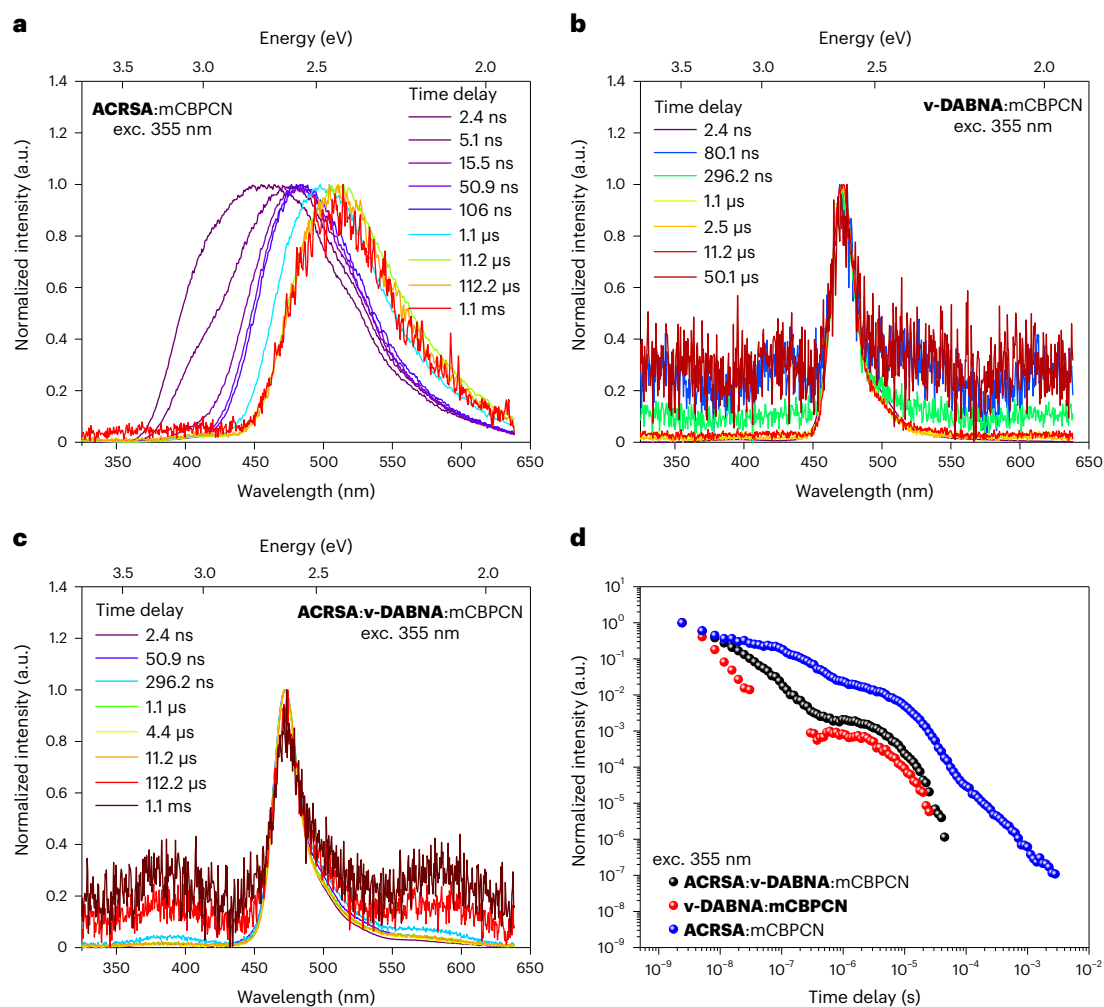


Fig. 2 | Time-resolved emission measurements following the exciton dynamics. **a–c**, Time-resolved PL spectra of **ACRSA:mCBPCN** (10%) (**a**), **v-DABNA:mCBPCN** (1%) (**b**) and **ACRSA:v-DABNA:mCBPCN** (10:1:89 wt%) (**c**). The DF lifetime of 10 wt% **ACRSA:mCBPCN** is 7.9 μ s because of the excimer states. For comparison, **ACRSA** at 1 wt% loading in zeonex or bis[2-(diphenylphosphino)phenyl]ether oxide (DPEPO) films have DF lifetimes of 6.3 and 7.3 μ s, respectively, with no excimer emission observed. At 10 wt% in DPEPO, similar to the mCBPCN host, the **ACRSA** DF lifetime is 8.7 μ s with a clear excimer emission observed³⁶. The excimer emission is not observed in the **ACRSA:v-DABNA:mCBPCN**

(10:1:89 wt%) delayed emission. **d**, PL decay traces of the evaporated films at room temperature. With the additional presence of 1 wt% **v-DABNA** (in the **ACRSA:mCBPCN** system), the PF lifetime has two components; directly excited **v-DABNA** with a lifetime of 3.5 ns, which is the same as **v-DABNA** in mCBPCN, and **ACRSA** excitation followed by FRET to **v-DABNA** with an average lifetime of 39.27 ns. Exciting the HF film at 420 nm to selectively excite **v-DABNA** produces the same emission decay kinetics as a film without the **ACRSA** sensitizer (Supplementary Fig. 3). Here $\lambda_{\text{exc}} = 355$ nm.

Table 1 | Key photophysical characteristics of ACRSA:v-DABNA:mCBPCN, ACRSA:mCBPCN and v-DABNA:mCBPCN films at room temperature ($\lambda_{\text{exc}} = 355$ nm)

Photophysical characteristics	ACRSA:vDABNA: mCBPCN (HF)	ACRSA:mCBPCN (sensitizer only)	v-DABNA:mCBPCN (terminal emitter only)
Concentration (wt%)	10:1:89	10:90	1:99
^a λ_{max} (nm)	476	500	477
^a Full-width at half-maximum (nm)	17.7	96.1	17.5
^b Φ_{PL} (%)	66.1	30.7	60.9
^c τ_{LE} host (ns)	3.5 (v-DABNA)	2.95	–
^c $\tau_{\text{PF},1}$ (ns)/(A _{PF})	15.99 (78%)	72.1 (60%)	3.5
^c $\tau_{\text{PF},2}$ (ns)	60.93 (22%)	391.14 (40%)	–
^d $\tau_{\text{PF,av}}$ (ns)	39.27	322.03	3.5
^c τ_{DF} (μ s)	4.5	7.9	4.6

^aValues were obtained from the steady-state PL spectra ^bPLQY (Φ_{PL}) under N_2 , excited at 355 nm ^cLifetimes were obtained by fitting monoexponential and biexponential functions ^dAverage lifetime $\tau_{\text{PF,av}} = (A_{\text{PF},1} \times \tau_{\text{PF},1}^2 + A_{\text{PF},2} \times \tau_{\text{PF},2}^2) / (A_{\text{PF},1} \times \tau_{\text{PF},1} + A_{\text{PF},2} \times \tau_{\text{PF},2})$.

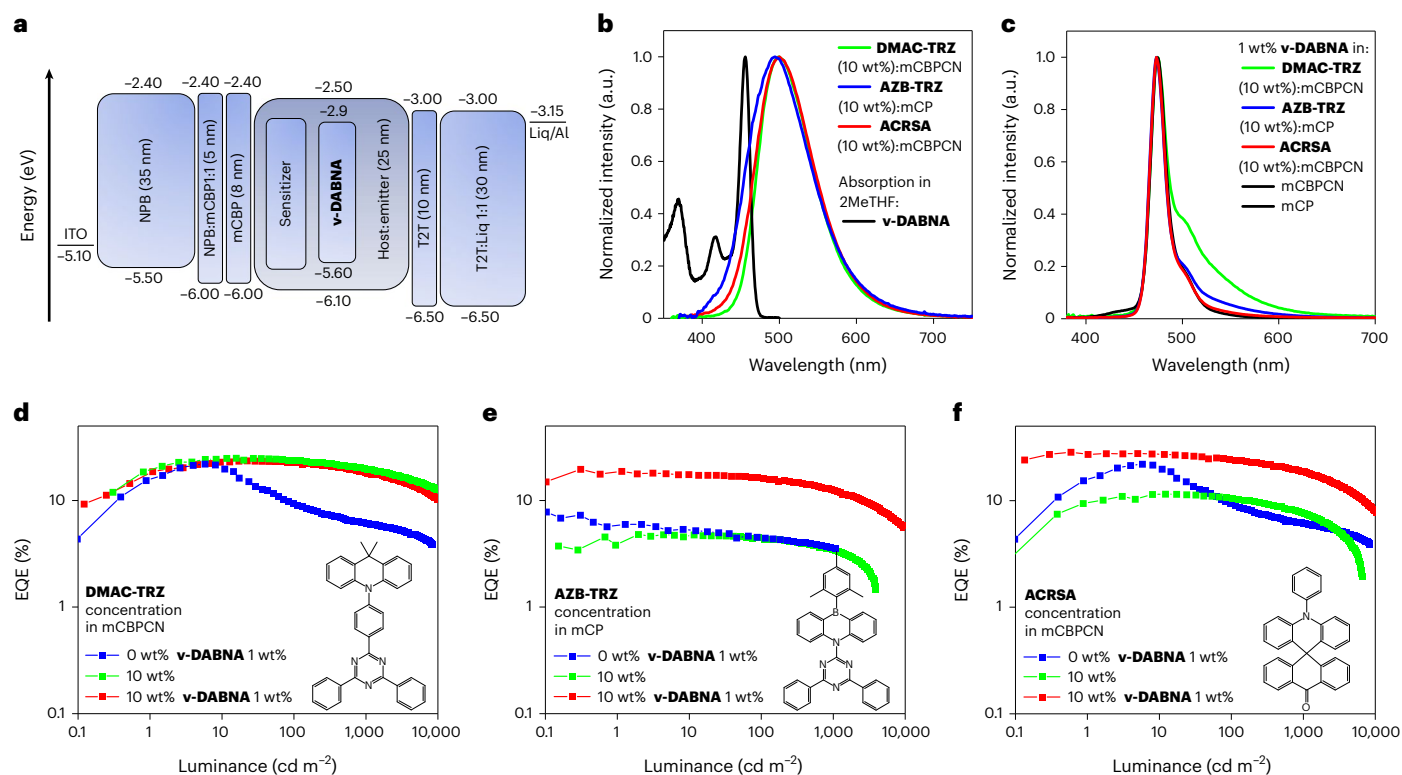


Fig. 4 | OLEDs. **a–c**, Device architecture (**a**) and EL spectra of TADF devices (**b**) and HF-OLEDs (**c**). A virtually complete FRET is observed in the **ACRSA** HF-OLEDs that have the EL spectra identical to those of **v-DABNA**. Conversely, residual sensitizer emission is observed (on the red side of the EL emission) in the

DMAC-TRZ and **AZB-TRZ** HF-OLEDs. **d–f**, EQE versus luminance of **DMAC-TRZ** (**d**), **AZB-TRZ** (**e**) and **ACRSA** (**f**) OLEDs with and without the terminal emitter (blue curve for **v-DABNA** without the presence of the sensitizer is shown for comparison).

The **ACRSA** emission and **v-DABNA** absorption overlap is small (Fig. 1), but this does not limit η_{FRET} . This crucial realization allows us to maintain efficient cumulative FRET as the excited-state energy of the sensitizer is minimized. This is not unique to **ACRSA**, but arises from the long excited-state lifetime so that the singlet excited-state population primarily resides in the S_1 zeroth vibrational level (Fig. 3). In **v-DABNA**, the S_0 – S_1 transition has very high oscillator strength and narrow bandwidth. Thus, the overlap between the sensitizer populated states and the spectrally narrow **v-DABNA** remains suitably strong, making the **ACRSA**:**v-DABNA** HF system ideal for maximal η_{FRET} despite the minimal spectral overlap. From this, surprisingly low sensitizer singlet and triplet excited-state energies can be used to sensitize blue terminal emitters, considerably increasing the range of usable low-energy hosts and emitter materials. This realization redefines the photophysical design requirements for sensitizer and terminal emitters to achieve optimal FRET alongside minimal sensitizer excited-state energies in HF-OLEDs.

Devices

OLEDs were fabricated using the same device architecture for all the devices as the sensitizers used have similar highest occupied molecular orbital and lowest unoccupied molecular orbital values. (Fig. 4a). Although device performance could improve in devices individually optimized for each emitter, comparing the sensitizer, terminal emitter and HF combinations in the same device structure provides an insight into the sensitization processes in each emitter.

It is well established that the slow rISC of multiresonance TADF materials such as **v-DABNA** leads to unsatisfactory efficiency roll-off at higher current densities in non-triplet-harvesting host devices^{20,21} (Fig. 4d–f, blue curve). We note that **v-DABNA** performs exceptionally well in a DOBNA-OAR host, but this is not well understood⁴¹. **ACRSA** does not perform as well in OLEDs as **DMAC-TRZ** (refs. 10,32). In our

device stack, the EQE_{max} value is limited to ~11% compared with ~25% for **DMAC-TRZ** (10 wt% sensitizer in the mCBPCN host). The roll-off for **ACRSA** is also worse than **DMAC-TRZ** OLEDs, a result of its slower rISC and longer exciton lifetimes (Supplementary Table 4). However, introducing 1 wt% **v-DABNA** to the **ACRSA** devices, the EQE_{max} almost triples to 28.5%, whereas **DMAC-TRZ**:**v-DABNA** HF-OLEDs show little change (Fig. 4). Furthermore, FRET is virtually complete in the **ACRSA** HF-OLEDs (Fig. 4c).

We propose that this remarkable performance enhancement in **ACRSA** HF-OLEDs arises from the same properties that make **ACRSA** a less effective TADF emitter. In particular, the slow radiative and non-radiative rates of **ACRSA** are extensively outcompeted by FRET to **v-DABNA**, overcoming its low PLQY. This long energy transfer window as well as the absence of any unfavourable conformers with poor η_{FRET} supports complete **ACRSA**:**v-DABNA** FRET. In contrast, k_{ISC} and k_{F} are comparably faster in **DMAC-TRZ**, leading to less complete FRET despite similar spectral overlap (Supplementary Table 3). The high PLQY in **DMAC-TRZ** means that radiative decay already outcompetes non-radiative decay, and therefore, the FRET processes cannot further improve the device performance. There also exists a sub-population of **DMAC-TRZ** molecules in unfavourable dihedral-angle configurations with redshifted emission inaccessible for FRET (Fig. 4c).

The similar EQE roll-off in the **ACRSA** TADF and HF devices indicate that triplet harvesting remains the exclusive role of the sensitizer, not the **v-DABNA** terminal emitter (Supplementary Table 7). The possibility of device degradation during the J – V – L measurements is excluded by the identical consecutive sweeps of the same pixel (Supplementary Fig. 11). Nonetheless, the roll-off slope is improved at high luminance, indicating that the HF-OLED probably reduces the accumulation of **ACRSA** excitons through rapid FRET. The demonstrated devices open a new path for blue OLEDs, through which deep-blue sensitizers and

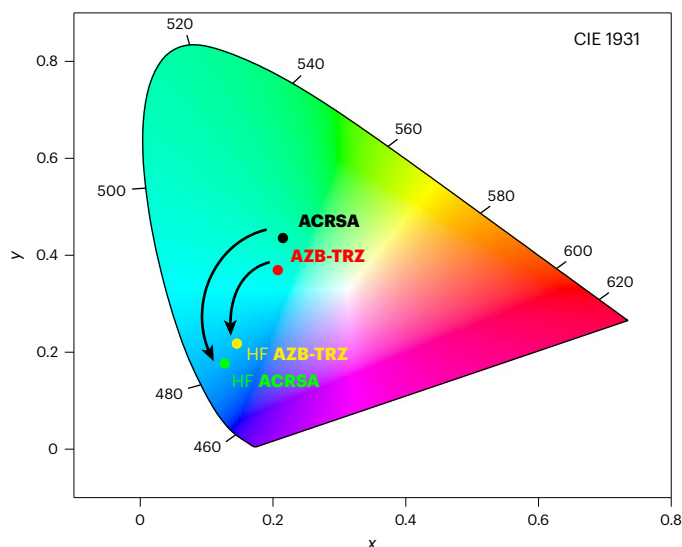


Fig. 5 | Comparison of CIE coordinates of ACRSA and AZB-TRZ OLEDs and HF-OLEDs. The ACRSA sensitizer giving the most complete energy transfer to the terminal emitter shows the largest blueshift in the colour coordinates to virtually that of the **v-DABNA:mCBPCNOLED**. The EL spectra are collected at $1,000 \text{ cd m}^{-2}$.

associated high triplet hosts are not necessary^{4,5,15}. Green-emitting TADF sensitizers with lower-triplet hosts can instead be used (offering substantially better stability in devices); combined with a highly absorbing red edge terminal emitter, these surprisingly effective HF systems with seemingly inadequate FRET overlap demonstrate an unexpected path to highly efficient blue OLEDs.

Supplementary Fig. 12 provides the stability of these devices. Surprisingly, the LT_{50} value for **DMAC-TRZ** OLEDs (at $1,500 \text{ cd m}^{-2}$) is four times longer than the corresponding HF-OLEDs (34.0 to 8.5 h). However, the opposite trend occurs in **ACRSA**-based devices, in which the lifetime improves by 2.5 times in HF-OLEDs (28 to 69 min at $2,500 \text{ cd m}^{-2}$), following efficient FRET and EQE improvements.

To explore this strategy further, we investigated an additional non-rigid TADF molecule, with blueshifted emission compared with **DMAC-TRZ**. **AZB-TRZ** (Fig. 4e) has fast non-radiative decay rate, fast k_{ISC} and low PLQY compared with **DMAC-TRZ** (Supplementary Table 2)³³. Similar to **DMAC-TRZ**, a clear distribution of dihedral angles is observed through the time-dependent emission spectra (Supplementary Fig. 5a), giving redshifted emission with limited spectral overlap to **v-DABNA**. Nonetheless, the spectral overlap is higher compared with **ACRSA** and **DMAC-TRZ** sensitizers (Supplementary Fig. 4), giving the highest J factor and FRET radius (Supplementary Tables 3 and 6) in this series of sensitizers.

Unsurprisingly, the CT energy dispersion together with fast k_{F} and k_{ISC} of **AZB-TRZ** compete with k_{FRET} (Supplementary Table 6), leading to a seemingly low η_{FRET} of 37%, but a high triplet population. The latter indicates why η_{FRET} appears to be underestimated; the HF-OLED spectra indicate near-complete energy transfer, that is, a small contribution from the sensitizer in the EL spectrum ($\sim 510 \text{ nm}$; Fig. 4c). Intersystem crossing/rISC cycling can efficiently harvest the high triplet population and FRET occurs throughout the DF/triplet regime, giving a larger cumulative η_{FRET} .

The combination of FRET and fast rISC, therefore, helps to greatly enhance the **AZB-TRZ** HF device efficiency, but the energy transfer is not as complete as in **ACRSA**. The fast radiative and non-radiative singlet decay rates do not allow FRET to completely dominate the exciton dynamics in **AZB-TRZ** HF devices, and their colour coordinates do not shift as much as that in **ACRSA** HF-OLEDs, despite **AZB-TRZ** having a higher energy emission and spectral overlap (Fig. 5). The

device EQE_{max} , nonetheless, quadruples from 5% to 20%, and the already excellent roll-off from rapid rISC in **AZB-TRZ** devices is enhanced in HF devices.

The power and current efficiencies of both **ACRSA** and **AZB-TRZ** HF-OLEDs show enhancement (Supplementary Figs. 7 and 8), only partially explained by the improved quantum efficiencies. In **ACRSA**, they rise from 31 cd A^{-1} and 28 lm W^{-1} in the greenish TADF OLEDs to 37 cd A^{-1} and 36 lm W^{-1} in the deeper-blue HF-OLEDs (Supplementary Table 7). The effect is even greater for **AZB-TRZ** HF-OLEDs, rising from 12 cd A^{-1} and 9 lm W^{-1} in TADF OLEDs to 30 cd A^{-1} and 27 lm W^{-1} in HF-OLEDs (Supplementary Fig. 8). In contrast, **DMAC-TRZ** HF-OLEDs show a decrease in power efficiency as EQE remains unchanged and only the spectrum changes (Supplementary Fig. 9). Considering the eye spectral response, a green emitter with similar radiance to a deeper-blue emitter will always have higher power efficiency—a trend that the overwhelming efficiency enhancements of our HF-OLEDs disrupts.

Discussion

We have elucidated key photophysical parameters that yield optimal triplet upconversion sensitization in HF-OLEDs. We show that these parameters considerably differ from those required for an efficient non-HF-TADF OLED emitter. Importantly, rigid TADF molecules with homogeneous CT emission energy, exemplified by the spiro-linked TADF molecule **ACRSA**, allow all the molecules in the film to undergo efficient, complete FRET. Long radiative lifetimes and low intersystem crossing rates are ideal for sensitization, allowing small spectral overlaps to achieve efficient cumulative FRET to the terminal emitter. High rISC (and consequently high intersystem crossing) rates remain desirable for fast triplet-harvesting and minimal triplet annihilation/quenching phenomena in TADF OLEDs. In HF-OLEDs, a much slower k_{ISC} and k_{r} can still support efficient sensitization if they can strike a delicate balance between being fast enough to ensure device stability and slow enough to allow FRET to outcompete the sensitizer's radiative and non-radiative processes, removing the need for high sensitizer PLQY. This strategy also enables the sensitizer excitation energies to be pushed lower and retaining deep-blue terminal emission, with substantial benefits on the choice of host material and device longevity.

These results reveal an interesting blind spot in TADF HF research. By limiting the scope to only the best-performing TADF materials as sensitizers, that is, **DMAC-TRZ**, many excellent HF pairs using 'less ideal' TADF sensitizers have probably been overlooked, and would probably never be considered or discovered. Because of this ability to turn intrinsically 'poor' TADF emitters into blue HF-OLEDs with exceptional performance (Supplementary Fig. 10), a re-evaluation of many previously reported and unreported TADF materials should be stimulated.

Online content

Any methods, additional references, Nature Portfolio reporting summaries, source data, extended data, supplementary information, acknowledgements, peer review information; details of author contributions and competing interests; and statements of data and code availability are available at <https://doi.org/10.1038/s41566-024-01395-1>.

References

1. On the way to becoming the world market leader in the OLED sector; <https://www.techtag.de/digitalisierung/digitale-pioniere/cynora-auf-dem-weg-zum-weltmarktfuehrer-im-oled-bereich-interview/>
2. Hong, G. et al. A brief history of OLEDs—emitter development and industry milestones. *Adv. Mater.* **33**, 2005630 (2021).
3. Samsung Display researching phosphorescent blue OLED material; <https://www.thelec.net/news/articleView.html?idxno=4044>

4. Ihn, S. et al. Dipole moment- and molecular orbital-engineered phosphine oxide-free host materials for efficient and stable blue thermally activated delayed fluorescence. *Adv. Sci.* **9**, 2102141 (2022).
5. Wright, I. A. et al. Conformational dependence of triplet energies in rotationally hindered *N*- and *S*-heterocyclic dimers: new design and measurement rules for high triplet energy OLED host materials. *Chem. Eur. J.* **27**, 6545–6556 (2021).
6. Aksoy, E., Danos, A., Varlikli, C. & Monkman, A. P. Navigating CIE space for efficient TADF downconversion WOLEDs. *Dyes Pigm.* **183**, 108707 (2020).
7. Monkman, A. Why do we still need a stable long lifetime deep blue OLED emitter? *ACS Appl. Mater. Interfaces* **14**, 20463–20467 (2022).
8. Baldo, M. A., Thompson, M. E. & Forrest, S. R. High-efficiency fluorescent organic light-emitting devices using a phosphorescent sensitizer. *Nature* **403**, 750–753 (2000).
9. Haase, N. et al. Are the rates of Dexter transfer in TADF hyperfluorescence systems optically accessible? *Mater. Horiz.* **8**, 1805–1815 (2021).
10. Nakanotani, H. et al. High-efficiency organic light-emitting diodes with fluorescent emitters. *Nat. Commun.* **5**, 4016 (2014).
11. Abroshan, H. et al. Thermally activated delayed fluorescence sensitization for highly efficient blue fluorescent emitters. *Adv. Funct. Mater.* **30**, 2005898 (2020).
12. Furukawa, T., Nakanotani, H., Inoue, M. & Adachi, C. Dual enhancement of electroluminescence efficiency and operational stability by rapid upconversion of triplet excitons in OLEDs. *Sci. Rep.* **5**, 8429 (2015).
13. Fukagawa, H., Shimizu, T., Iwasaki, Y. & Yamamoto, T. Operational lifetimes of organic light-emitting diodes dominated by Förster resonance energy transfer. *Sci. Rep.* **7**, 1735 (2017).
14. Hatakeyama, T. et al. Ultrapure blue thermally activated delayed fluorescence molecules: efficient HOMO-LUMO separation by the multiple resonance effect. *Adv. Mater.* **28**, 2777–2781 (2016).
15. Stavrou, K. et al. Emission and absorption tuning in TADF B,N-doped heptacenes: toward ideal-blue hyperfluorescent OLEDs. *Adv. Opt. Mater.* **10**, 2200688 (2022).
16. Alam, M. I. et al. Acceptor interlocked molecular design for solution-processed stable deep-blue TADF and hyperfluorescence organic LED enabling high-efficiency. *Adv. Opt. Mater.* **10**, 2200376 (2022).
17. Stavrou, K. et al. Unexpected quasi-axial conformer in thermally activated delayed fluorescence DMAC-TRZ, pushing green OLEDs to blue. *Adv. Funct. Mater.* **33**, 2300910 (2023).
18. Wada, Y., Nakagawa, H., Matsumoto, S., Wakisaka, Y. & Kaji, H. Organic light emitters exhibiting very fast reverse intersystem crossing. *Nat. Photon.* **14**, 643–649 (2020).
19. Kim, J. H., Lee, K. H. & Lee, J. Y. Design of thermally activated delayed fluorescent assistant dopants to suppress the nonradiative component in red fluorescent organic light-emitting diodes. *Chem. Eur. J.* **25**, 9060–9070 (2019).
20. Jeon, S. O. et al. High-efficiency, long-lifetime deep-blue organic light-emitting diodes. *Nat. Photon.* **15**, 208–215 (2021).
21. Chan, C.-Y. et al. Stable pure-blue hyperfluorescence organic light-emitting diodes with high-efficiency and narrow emission. *Nat. Photon.* **15**, 203–207 (2021).
22. Lee, Y. et al. Investigating HOMO energy levels of terminal emitters for realizing high-brightness and stable TADF-assisted fluorescence organic light-emitting diodes. *Adv. Electron. Mater.* **7**, 2001090 (2021).
23. Naveen, K. R. et al. Achieving high efficiency and pure blue color in hyperfluorescence organic light emitting diodes using organo-boron based emitters. *Adv. Funct. Mater.* **32**, 2110356 (2022).
24. Naveen, K. R., Palanisamy, P., Chae, M. Y. & Kwon, J. H. Multiresonant TADF materials: triggering the reverse intersystem crossing to alleviate the efficiency roll-off in OLEDs. *Chem. Commun.* **59**, 3685–3702 (2023).
25. Naveen, K. R., Yang, H. I. & Kwon, J. H. Double boron-embedded multiresonant thermally activated delayed fluorescent materials for organic light-emitting diodes. *Commun. Chem.* **5**, 149 (2022).
26. Cheng, Y. et al. A highly twisted carbazole-fused DABNA derivative as an orange-red TADF emitter for OLEDs with nearly 40% EQE. *Angew. Chem. Int. Ed.* **61**, e202212575 (2022).
27. Stavrou, K., Danos, A., Hama, T., Hatakeyama, T. & Monkman, A. Hot vibrational states in a high-performance multiple resonance emitter and the effect of excimer quenching on organic light-emitting diodes. *ACS Appl. Mater. Interfaces* **13**, 8643–8655 (2021).
28. Naqvi, B. A. et al. What controls the orientation of TADF emitters? *Front. Chem.* **8**, 750 (2020).
29. Penfold, T. J., Dias, F. B. & Monkman, A. P. The theory of thermally activated delayed fluorescence for organic light emitting diodes. *Chem. Commun.* **54**, 3926–3935 (2018).
30. Kukhta, N. A. et al. Revealing resonance effects and intramolecular dipole interactions in the positional isomers of benzonitrile-core thermally activated delayed fluorescence materials. *J. Mater. Chem. C* **7**, 9184–9194 (2019).
31. Tsai, W.-L. et al. A versatile thermally activated delayed fluorescence emitter for both highly efficient doped and non-doped organic light emitting devices. *Chem. Commun.* **51**, 13662–13665 (2015).
32. Nasu, K. et al. A highly luminescent spiro-anthracenone-based organic light-emitting diode exhibiting thermally activated delayed fluorescence. *Chem. Commun.* **49**, 10385–10387 (2013).
33. Sudhakar, P. et al. Azaborine as a versatile weak donor for thermally activated delayed fluorescence. *ACS Appl. Mater. Interfaces* **15**, 25806–25818 (2023).
34. Stavrou, K., Franca, L. G. & Monkman, A. P. Photophysics of TADF guest–host systems: introducing the idea of hosting potential. *ACS Appl. Electron. Mater.* **2**, 2868–2881 (2020).
35. Kelly, D., Franca, L. G., Stavrou, K., Danos, A. & Monkman, A. P. Laplace transform fitting as a tool to uncover distributions of reverse intersystem crossing rates in TADF systems. *J. Phys. Chem. Lett.* **13**, 6981–6986 (2022).
36. Franca, L. G., Danos, A. & Monkman, A. Spiro donor–acceptor TADF emitters: naked TADF free from inhomogeneity caused by donor acceptor bridge bond disorder. Fast rISC and invariant photophysics in solid state hosts. *J. Mater. Chem. C* **10**, 1313–1325 (2022).
37. Franca, L. G., Danos, A. & Monkman, A. Donor, acceptor, and molecular charge transfer emission all in one molecule. *J. Phys. Chem. Lett.* **14**, 2764–2771 (2023).
38. Tsuchiya, Y. et al. Exact solution of kinetic analysis for thermally activated delayed fluorescence materials. *J. Phys. Chem. A* **125**, 8074–8089 (2021).
39. Sem, S. et al. Determining non-radiative decay rates in TADF compounds using coupled transient and steady state optical data. *J. Mater. Chem. C* **10**, 4878–4885 (2022).
40. *FRET—Förster Resonance Energy Transfer* (Wiley, 2013).
41. Kondo, Y. et al. Narrowband deep-blue organic light-emitting diode featuring an organoboron-based emitter. *Nat. Photon.* **13**, 678–682 (2019).

Publisher's note Springer Nature remains neutral with regard to jurisdictional claims in published maps and institutional affiliations.

Open Access This article is licensed under a Creative Commons Attribution 4.0 International License, which permits use, sharing, adaptation, distribution and reproduction in any medium or format, as long as you give appropriate credit to the original author(s) and the source, provide a link to the Creative Commons license, and indicate if changes were made. The images or other third party material in this article are included in the article's Creative Commons license, unless indicated otherwise in a credit line to

the material. If material is not included in the article's Creative Commons license and your intended use is not permitted by statutory regulation or exceeds the permitted use, you will need to obtain permission directly from the copyright holder. To view a copy of this license, visit <http://creativecommons.org/licenses/by/4.0/>.

© The Author(s) 2024

Methods

Photophysical measurements

Solid-state samples were evaporated on quartz substrates into a Kurt J. Lesker Super Spectros deposition chamber, at pressures below 10^{-7} mbar. Steady-state absorption and emission spectra were measured using a double-beam Shimadzu UV-3600 UV/VIS/NIR spectrophotometer and a Horiba Jobin Yvon Fluorolog-3 spectrofluorometer, respectively. Time-resolved measurements were performed using a spectrograph (Horiba Triax) and a Stanford Computer Optics 4 Picos intensified charge-coupled device camera, where samples were excited with a Nd:YAG laser (EKSPLA, 10 Hz, 355 nm) under a vacuum.

Device fabrication

OLEDs were fabricated on patterned indium-tin-oxide-coated glass (VisionTek Systems) with a sheet resistance of $15 \Omega \text{ sq}^{-1}$. After sonicating in acetone and isopropanol, oxygen-plasma-cleaned substrates were loaded into a Kurt J. Lesker Super Spectros deposition chamber, and both small-molecule and cathode layers were thermally evaporated at pressures below 10^{-7} mbar. The materials used for the production of the OLEDs were *N,N*-bis(naphthalene-1-yl)-*N*,*N*-bis(phenyl)benzidine (NPB) as the hole transport layer; 3,3'-di(9H-carbazol-9-yl)-1,1'-biphenyl (mCBP) as the electron blocking layer; the emission layer had mCBPCN or 1,3-bis(*N*-carbazolyl)benzene (mCP) as the host, **DMAC-TRZ**, **ACRSA** and **AZB-TRZ** as the sensitizer, **v-DABNA** as the terminal emitter, 2,4,6-tris(biphenyl-3-yl)-1,3,5-triazine (T2T) as the hole blocking layer, T2T and 8-hydroxyquinolinolato-lithium (LiQ) as the electron transport/injection layer and an aluminium (Al) cathode. NPB, mCP, mCBP and T2T were purchased from Sigma-Aldrich, and mCBPCN and **ACRSA** were purchased from Ossila; they were sublimed before use. Sublimed **DMAC-TRZ** was purchased from Lumtec. **v-DABNA** was synthesized and purified by T. Hatakeyama's group. **AZB-TRZ** was synthesized and purified by E. Zysman-Colman's group.

Device characterization

Freshly evaporated devices were transferred into a calibrated six-inch integrating sphere (Labsphere) in a glovebox, and their electrical properties were measured using a source meter (Keithley 2400). The emission spectra were simultaneously measured using both calibrated fibre-coupled spectrometer (Ocean Optics USB4000) and photodiode, for low luminance. All the devices were evaluated at 293 K and under a N_2 atmosphere.

Device lifetime

The OLED lifetime measurements were measured in a glovebox under a N_2 atmosphere using an Ossila LED Measurement System.

Data availability

The data that support the plots within this paper and the Supplementary Information and other findings of this study are available from the corresponding authors upon reasonable request.

Acknowledgements

We thank T. Hatakeyama and E. Zysman-Colman for providing the **v-DABNA** and **AZB-TRZ** emitters, respectively. K.S. and L.G.F. acknowledge the European Union's Horizon 2020 research and innovation programme for funding under the Marie Skłodowska-Curie grant agreement no. 812872 (TADFLife). A.P.M. acknowledges the EPSRC for funding under grant no. EP/TO2240X/1.

Author contributions

K.S. and A.P.M. conceived the idea. K.S. designed the experiments. K.S. performed the photophysics, FRET calculations, device fabrication and analysis. K.S. and L.G.F. conducted the time-resolved PL measurements. A.D. measured the PLQY. All authors contributed to the discussion, writing and editing of the manuscript. A.P.M. supervised the project.

Competing interests

The authors declare no competing interests.

Additional information

Supplementary information The online version contains supplementary material available at <https://doi.org/10.1038/s41566-024-01395-1>.

Correspondence and requests for materials should be addressed to Kleitos Stavrou or Andrew P. Monkman.

Peer review information *Nature Photonics* thanks Hironori Kaji, Zhongjie Ren and the other, anonymous, reviewer(s) for their contribution to the peer review of this work.

Reprints and permissions information is available at www.nature.com/reprints.